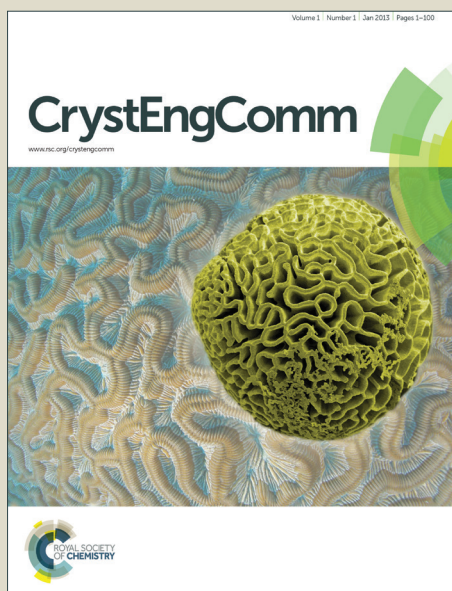


# CrystEngComm

Accepted Manuscript



This is an *Accepted Manuscript*, which has been through the Royal Society of Chemistry peer review process and has been accepted for publication.

*Accepted Manuscripts* are published online shortly after acceptance, before technical editing, formatting and proof reading. Using this free service, authors can make their results available to the community, in citable form, before we publish the edited article. We will replace this *Accepted Manuscript* with the edited and formatted *Advance Article* as soon as it is available.

You can find more information about *Accepted Manuscripts* in the [Information for Authors](#).

Please note that technical editing may introduce minor changes to the text and/or graphics, which may alter content. The journal's standard [Terms & Conditions](#) and the [Ethical guidelines](#) still apply. In no event shall the Royal Society of Chemistry be held responsible for any errors or omissions in this *Accepted Manuscript* or any consequences arising from the use of any information it contains.

*Submitted to CrystEngComm*

# **Thermodynamics and preliminary pharmaceutical characterization of melatonin–pimelic acid cocrystal prepared by a melt crystallization method**

Yan Yan<sup>a,b</sup>, Jia-Mei Chen<sup>a,\*</sup>, Tong-Bu Lu<sup>a,b</sup>

<sup>a</sup> *School of Pharmaceutical Sciences, Sun Yat-Sen University, Guangzhou, China*

<sup>b</sup> *MOE Key Laboratory of Bioinorganic and Synthetic Chemistry / School of Chemistry and Chemical Engineering, Sun Yat-Sen University, Guangzhou, China*

†Electronic supplementary information (ESI) available: CCDC reference number 1024880 for melatonin–pimelic acid cocrystal.

\* Corresponding author. Tel.: + 86 20 84112921; fax: +86 20 84112921.

*E-mail address:* chenjm37@mail.sysu.edu.cn (J. M. Chen).

**ABSTRACT**

Pharmaceutical cocrystals have been extensively investigated as a promising approach to improve drugs' physicochemical properties. Cocrystals are usually prepared from solution-mediated methods and grinding methods. In this study, a cocrystal of pimelic acid with poorly soluble melatonin was produced by a melt crystallization method with control of crystallization within a specific temperature range. The cocrystal was characterized by infrared spectra, powder and single crystal X-ray diffraction. The binary phase diagram and the formation enthalpy established by differential scanning calorimetry provided the rationale for this spontaneous cocrystallization system. The cocrystal exhibited higher apparent solubility, faster dissolution rate and acceptable stability as compared to original melatonin. The study has shown that the melt crystallization method can be considered as a competitive route for producing pharmaceutical cocrystals with improved properties and the thermodynamic investigation can provide in depth understanding and guidance during melt crystallization of cocrystals.

## Introduction

Pharmaceutical cocrystals can be defined as crystalline materials that composed of an active pharmaceutical ingredient (API) and one or more pharmaceutically acceptable compounds (guests, coformers) , usually held together by reliable hydrogen bonding interactions, in the same crystal lattice.<sup>1-3</sup> The molecular packing rearrangements of APIs in cocrystals are facilitated by the introduction of guest molecules into the crystal lattice, which result in modification of their relevant physicochemical properties. Thus, pharmaceutical cocrystals provide new opportunities to enhance the physicochemical properties, such as melting point, hygroscopicity, mechanical properties, permeability, solubility, dissolution rate, and bioavailability, of APIs.<sup>4-11</sup> In addition, cocrystal formation may also create the intellectual property and new patents of APIs for extending their life cycle in the pharmaceutical industry.<sup>12</sup> Hence, pharmaceutical cocrystals have drawn great attention from both academia and industry evidenced by the growing number of research publications and patent applications.<sup>4-12</sup>

Cocrystals are usually prepared from solution-mediated methods (including solvent evaporation, reaction crystallization, slurring, or anti-solvent addition, etc.).<sup>13-17</sup> This approach, however, is limited by the time-consuming solvent selection process, the potential for single component crystallization and solvate formation. Solid-based methods (neat or solvent-assisted grinding) have also been demonstrated as effective methodologies for the preparation of cocrystals.<sup>13,18</sup> Grinding methods often need the special equipment to keep the grinding frequency, and the resulting products often contain amorphous impurity. Additionally, thermal methods (Kofler technique, co-melting or melt crystallization), which is long known but rarely used in cocrystal systems, is a green alternative approach to identifying cocrystal phases.<sup>19-22</sup> This approach could only be applied for thermally stable compounds with appropriate melting

point. The choice of cocrystallization techniques in the cocrystal screening depends on the specific properties of the starting materials, including solubility, crystalline, melting point, thermal stability, etc.

Melatonin (MT, Fig. 1) (N-acetyl-5-methoxytryptamine) is a natural product, and is found in the pineal gland and excreted as a hormone in humans.<sup>23</sup> It is produced in the brain that helps regulate the sleep and wake cycle.<sup>24</sup> Exogenous MT is used orally for jet lag, insomnia, shift-work disorder, circadian rhythm disorders in the blind, and benzodiazepine and nicotine withdrawal.<sup>25</sup> In most countries MT preparations are available as food supplements.<sup>26</sup> A prescription-only MT product was approved for use by the European Medicines Agency in 2007.<sup>27</sup> MT belongs to class II of the biopharmaceutics classification system (BCS) with low solubility and high permeability.<sup>28,29</sup> The oral bioavailability of MT in human is limited and variable.<sup>30</sup> Consequently, improving the solubility of MT is highly desirable.

Herein we attempt to address the deficiency in solubility for MT by cocrystallization with soluble guest molecules. Formation of a cocrystal requires complementary hydrogen bonding between MT and a second molecule. The most useful hydrogen bonding group of MT is the secondary amide functionality, which is known to form robust hydrogen bonding interactions with carboxylic compounds.<sup>31,32</sup> A group of nontoxic carboxylic acids were used for cocrystal screening. Finally, only one cocrystal of MT with pimelic acid (PA, Fig. 1) was successfully obtained through a melt crystallization method and characterized by infrared spectra, powder and single crystal X-ray diffraction. Thermodynamics investigation and pharmaceutical characterization of MT–PA cocrystal were also carried out.

## Materials and methods

### Materials

MT was purchased from Hubei Yuancheng Pharmaceutical Co. Ltd. All of the cofomers were purchased from Aladdin reagent Inc. All of the other chemicals and solvents were commercially available and used as received.

### **Melt crystallization**

Melt crystallization method was employed to screen a total of 8 carboxylic acids and determine if unique cocrystalline phases with MT were able to form. In a typical experiment, a physical mixture of MT and each cofomer at a chosen ratio was heated at  $10\text{ }^{\circ}\text{C}\cdot\text{min}^{-1}$  until a melt was formed. The molten mixture was then cooled to different specific temperatures at a cooling rate of  $10\text{ }^{\circ}\text{C}\cdot\text{min}^{-1}$ . Then the mixture was stood at the temperature until crystallization process completed, which usually takes 10 to 24 h. The resulting solids were analyzed by X-ray diffraction for new crystalline phases. The results of the screen experiments are listed in Table 1 and Table 2.

### **Hot-stage microscopy (HSM)**

Thermomicroscopic investigations were performed with an optical polarizing microscope (Nikon LV100 POL) equipped with a Linkam hot-stage THMS 600 connected to a THMS 600 temperature controller and a LNP 95 liquid nitrogen pump. The microscopic images were recorded with a CCD camera attached to the Nikon LV100 POL microscope at every 10 s time intervals using Linksys 32 image capture software. A 1:1 MT/PA physical mixture were heated to  $130\text{ }^{\circ}\text{C}$ , and the temperature was kept until all the solids completely melted. Then the melt was cooled to  $50\text{ }^{\circ}\text{C}$  at a rate of  $10\text{ }^{\circ}\text{C}\cdot\text{min}^{-1}$ , and kept the temperature at  $50\text{ }^{\circ}\text{C}$  until the crystallization process completed.

### Preparation of single crystals of MT–PA cocrystal

The products obtained by melt crystallization were used as raw material for growing high-quality crystals from solution. Powder (20 mg) of MT–PA cocrystal was dissolved in mixed solvent of dichloromethane (1 mL) and n-hexane (0.6 mL). The resulting solution was allowed to evaporate slowly at room temperature and needle-like single crystals were obtained.

### Single crystal X-ray diffraction

Single crystal X-ray diffraction data for MT–PA cocrystal were collected on an Agilent Technologies Gemini A Ultra system with graphite monochromated Cu K $\alpha$  radiation ( $\lambda = 1.54178 \text{ \AA}$ ). Cell refinement and data reduction were applied using the program of CrysAlis PRO.<sup>33</sup> The structures were solved by the direct methods using the SHELX-97 program,<sup>34</sup> and refined by the full-matrix least-squares method on  $F^2$ . All non-hydrogen atoms were refined with anisotropic displacement parameters. Hydrogen positions on nitrogen and oxygen were located in Fourier-difference electron density maps. Hydrogen atoms associated with carbon atoms were refined in geometrically constrained riding positions. Crystallographic data and details of refinements are listed in Table 3, and hydrogen bonding distances and angles are given in Table 4.

### Powder X-ray diffraction (PXRD)

PXRD patterns were obtained on a Bruker D2 Phaser with Cu K $\alpha$  radiation ( $\lambda = 1.54178 \text{ \AA}$ ) at 30 kV and 10 mA. Data were recorded in the range of  $5 \sim 40^\circ (2\theta)$  in a continuous scan mode using a step size of  $0.014^\circ (2\theta)$  and a scan speed of 0.1 s/step.

### **Fourier-transform infrared spectroscopy (FTIR)**

FTIR spectra were recorded in the 4000 to 400  $\text{cm}^{-1}$  region using KBr pellets and a Bruker EQUINOX 55 spectrometer. A total 64 scans were collected with a resolution of 0.2  $\text{cm}^{-1}$  for each sample.

### **Differential scanning calorimetry (DSC)**

DSC was performed using a Netzsch 200 F3 Maja instrument. Samples were weighed out (1.8 ~ 2.5 mg) in aluminum sample pans and scanned from 30 to 130  $^{\circ}\text{C}$  under nitrogen atmosphere, with a heating rate of 5  $^{\circ}\text{C}\cdot\text{min}^{-1}$ .

### **Dissolution experiments**

Concentrations of MT were determined by a Cary 50 UV/vis spectrophotometry at 230 nm, where PA does not absorb and, therefore, did not interfere with determination of the concentration of MT. For experiments involving MT, MT-PA cocrystal and the 1:1 MT/PA physical mixture, absorbance values were related to concentrations of MT using a calibration curve.

For the powder dissolution experiments, all the solids were milled to powder and sieved using standard mesh sieves to provide samples with approximate particle size ranges of 75 ~150  $\mu\text{m}$ . In a typical experiment, a flask containing 300 mg of sample was added 50 mL of phosphate buffer saline (PBS, pH 6.8), and the resulting slurry was stirred at 37  $^{\circ}\text{C}$  and 500 rpm. At each time interval an aliquot of the slurry was withdrawn from the flask and filtered through a 0.22  $\mu\text{m}$  nylon filter. A 0.01 mL portion of the filtered aliquot was diluted to 1.0 mL with water and was

measured with UV/vis spectrophotometry. After the last aliquot was collected, the remaining solids were filtered, dried and analyzed by PXRD.

Intrinsic dissolution measurements were performed using the dissolution device ZQY-2 Dissolution Tester (Shanghai Huanghai Yaojian instrument distribution Co, Ltd.). In each experiment, 500 mL of PBS (pH 6.8) were equilibrated at 37.0 °C in a constant-temperature bath and stirred at 100 rpm. Approximately 150 mg of each solid was compressed in a hydraulic press at 1 ton for 5 seconds in a die of 5 mm diameter disk. The disks were coated using paraffin wax, leaving only the surface under investigation free for dissolution. These disks were immersed in the dissolution media, and at each time interval, 2 mL of solution was withdrawn and replaced by an equal volume of fresh medium to maintain a constant volume. The concentration of MT was measured with UV/vis spectrophotometry. Each intrinsic dissolution test lasted 60 min, after which time the disks were recovered, carefully ground and checked by PXRD. Finally, intrinsic dissolution rates were calculated from the slope of the linear regions of the dissolution curves.

### **Dynamic vapor sorption (DVS) Studies**

A DVS intrinsic instrument (Surface Measurement Systems, London, UK) was employed to investigate the hygroscopicity of MT, MT-PA cocrystal, and the physical mixture by measuring the uptake and loss of water vapor gravimetrically using an ultra sensitive recording microbalance with a mass resolution of  $\pm 0.1 \mu\text{g}$ . The temperature was maintained constant at  $25 \pm 0.1$  °C. For each sample, about 20 mg was loaded onto a metal sample pan and pre-equilibrated at 0 % RH in a continuous flow of dry nitrogen for several hours to establish the equilibrium dry mass. The relative humidity was then increased from 0 to 90 % in 10 % steps. For the desorption process, the RH was decreased in a similar manner. The equilibration criterion  $dm/dt$  (change in

mass as function of time) was set at 0.002 %/min for all steps. The sorption isotherms were calculated from the equilibrium mass values.

## Results and discussion

### Preparation of the cocrystal

A set of 8 pharmaceutically acceptable carboxylic acids were selected as potential cocrystal cofomers (Table 1). Crystallization experiments from solutions of MT and guest acids resulted in individual component phases because of their difference in solubility. As the selected carboxylic acids and MT are thermally stable compounds, we choose to use a cocrystal screening technique based on a melt crystallization method. Most carboxylic acids produced physical mixtures of the parental compounds when crystallizing from the molten mixtures with MT. Only one unique cocrystal of MT with PA (MT–PA cocrystal) was identified by appearance of new reflections in the diffractogram at 7.1, 25.6 ° ( $2\theta$ ) (Fig. 2), which do not exist in diffractograms of the starting materials.

Development of a robust procedure to prepare MT–PA cocrystal was proved to be non-trivial. In initial experiments, molten mixtures of MT and PA were allowed to cool to room temperature (RT) and to crystallize under this temperature, yielding only physical mixtures of individual components. To achieve a robust cocrystallization process, it is prerequisite to identify key factors affecting the melt crystallization between MT and PA. Thus a series of melt crystallization experiments at different MT/PA molar ratios and different temperatures were conducted (Table 2). PXRD patterns of the different MT/PA systems are presented in Fig. 2. When a molten mixture at a MT/PA molar ratio of 1:2 or 2:1 was cooled to 50 °C and allowed to crystallize completely, new peaks were observed other than those corresponding to the excess amounts of the starting components (Fig. 2), which indicated that 1:2 and 2:1 were unsuitable

stoichiometry for cocrystal formation. Meanwhile, no PXRD peaks indicative of the starting components were observed for the crystallization product with the 1:1 ratio (Fig. 2), thereby suggesting that the stoichiometry of the cocrystal was 1:1.

To further identify whether the temperature at which crystallization occur affects the outcome of melt crystallization, 1:1 MT/PA molten mixture was cooled to a series of specific temperature and then kept at each temperature until the crystallization process completed. We have tested the temperature from RT ( $\sim 25\text{ }^{\circ}\text{C}$ ) to  $80\text{ }^{\circ}\text{C}$  which is close to the melting point of MT-PA cocrystal. The cocrystal formation between MT and PA apparently occurred when allowed to crystallize under the temperature within the range of  $50\text{ }^{\circ}\text{C}$   $\sim 70\text{ }^{\circ}\text{C}$ . The crystallization behavior of the 1:1 molten mixture of MT/PA at  $50\text{ }^{\circ}\text{C}$  was observed by HSM (Fig. 3). Some needle-like crystals were found to appear from the amorphous phase under  $50\text{ }^{\circ}\text{C}$  after 10 min, and the whole crystallization process completed in 10 h. The physical mixtures of the components were obtained when controlling the crystallization within  $25\text{ }^{\circ}\text{C}$   $\sim 40\text{ }^{\circ}\text{C}$ , while it is possible to produce either the cocrystal or the physical mixture when crystallizing within  $40\text{ }^{\circ}\text{C}$   $\sim 50\text{ }^{\circ}\text{C}$ . Overall, the robust preparation method of phase pure MT-PA cocrystal is cooling 1:1 MT/PA molten mixture, with the control of crystallization temperature between  $50$  and  $70\text{ }^{\circ}\text{C}$ .

### Crystal structure analysis

The crystal structure analysis for MT-PA cocrystal was performed to identify the molecular interactions between MT and PA. The MT-PA cocrystal adopts the monoclinic P21/c space group, with one molecule each of MT and PA in the asymmetric unit (Table 3). To compare the hydrogen bonding models before and after cocrystal formation, the structures of pure MT and PA were analyzed from a crystal engineering perspective. Examination of the crystal structure of

MT (refcode MELATN01) reveals that the secondary amide group is the main hydrogen bond donor–acceptor functionality, which link MT molecules to form a one-dimensional chain through N–H...O hydrogen bonds (N...O, 2.963 Å; N–H...O, 161.62 °) (Fig. 4a). The crystal structure of PA (refcode PIMELA06) adopts a structural unit of carboxylic acid dimers via double O–H...O hydrogen bonds (O...O, 2.669 Å; O–H...O, 175.52 °) (Fig. 4b). After formation of MT–PA cocrystal, one carboxylic acid group of PA links to amide functionality of MT by a pair of O3–H3...O1 and N1–H1...O3 hydrogen bonds (O3...O1, 2.575(2) Å; O3–H3...O1, 164(4) °; N1...O3, 3.209(3) Å; N1–H1...O3, 175(2) °, Table 4) to form a one-dimensional chain. This carboxylic acid group also forms a strongly bent and thus weaker hydrogen bond (N2...O4, 3.055 Å; N2–H2...O4, 125 °) with the ring N–H donor of MT. The second acid group retains acid-acid dimer structural unit with double O6–H6...O5 hydrogen bonds (O...O, 2.660(2) Å; O–H...O, 172(3) °, Table 4), which make the one-dimensional aggregates propagate into a second dimension (Fig. 4c). The hydrogen bonding distance of amide increases from 2.963 Å in MT to 3.209(3) Å in MT–PA cocrystal. The hydrogen bonding angle of carboxylic acid decreases from 175.52 ° in PA to 164(4) ° in the cocrystal. These results indicate that as MT cocrystallizes with PA, the resulting structure fail to achieve stronger hydrogen bonding interactions, and the formed hydrogen bonds are weaker than those in the individual component phases.

### FTIR spectroscopy characteristics

The FTIR spectra for MT, PA and MT–PA cocrystal are presented to further verify the hydrogen bonded changes involved in the bulk cocrystal production (Fig. 5). MT shows the characteristic absorption peaks at 1630 and 3304  $\text{cm}^{-1}$ , which are assigned to C=O and N–H stretch of the secondary amide, respectively (Fig. 5a). It indicates that MT was the starting material in the

cocrystallization. The spectrum of PA has peaks corresponding to carboxylic C=O and O–H stretch at  $1689\text{ cm}^{-1}$  and  $2939\text{ cm}^{-1}$ , respectively (Fig. 5b). This suggests the structural units of hydrogen bonded carboxylic acid dimers being formed in the PA crystalline lattice.

The spectrum of MT–PA cocrystal has three distinctive peaks at  $1638$ ,  $1691$  and  $1711\text{ cm}^{-1}$ , which are assigned to the C=O stretch of the amide group in MT and two carboxylic acid groups in PA, respectively (Fig. 5c). The increase in the C=O stretching frequency from  $1630\text{ cm}^{-1}$  and  $1689\text{ cm}^{-1}$  in the component phases, respectively, to  $1638\text{ cm}^{-1}$  and  $1711\text{ cm}^{-1}$  in the cocrystal implies that the C=O groups are participating in weaker hydrogen bonds accompanying cocrystal formation. The O–H stretching frequency of PA and the N–H stretching frequency of MT were observed at  $3390$  and  $3435\text{ cm}^{-1}$ , respectively, in the cocrystal (Fig. 5c). A hypsochromic shift in the O–H and N–H stretching frequency further verifies the formation of weaker hydrogen bonds accompanying cocrystallization. These results from bulk cocrystal are consistent with the observations from single crystal structure analysis.

### **Thermodynamics of cocrystal formation**

After the characterization of the cocrystal, we attempted to investigate the thermodynamics of cocrystal formation. The temperature-composition phase diagram is an essential knowledge for any cocrystal system, as it indicates the phases formed at different compositions of the cocrystal formers over a range of temperatures. The phase diagrams of the MT–PA system was constructed by thermal analysis of corresponding binary mixtures using DSC (Fig. 6). The present study shows a representative phase diagram for a binary mixture forming a 1: 1 cocrystal with three local melting point maxima (i.e., for two pure components and the cocrystal), separated by two eutectics.<sup>35</sup> The diagram shows a congruent melting temperature of  $80.6\text{ }^{\circ}\text{C}$  at

mole fraction of 0.5, which is the melting point of MT–PA cocrystal and below those of MT (117.3 °C) and PA (107.1 °C). The two eutectics occurred at 71.1 °C and 78.9 °C, corresponding to the 0.37 and 0.65 mole fraction of MT, respectively.

The formation property of a cocrystal AB is defined in reference to Eq. (1):



where A, B, AB are the crystal of component A (MT) and component B (PA), and the cocrystal of A and B (MT–PA), respectively. Then the formation enthalpy of the cocrystal can be determined by Eq. (2),<sup>19,36</sup>

$$\Delta H_f = \Delta H_{m(\text{mix})}(T_s \rightarrow T_L) - \Delta H_{m(\text{cocrystal})}(T_s \rightarrow T_L) \quad (2)$$

where  $T_s$  is a temperature at which MT–PA cocrystal and the physical mixture of MT and PA are solid,  $T_L$  is a temperature at which the cocrystal and the physical mixture are both melted to the same liquid, and  $\Delta H_{m(\text{cocrystal})}(T_s \rightarrow T_L)$  and  $\Delta H_{m(\text{mix})}(T_s \rightarrow T_L)$  are the corresponding enthalpies of melting. Table 5 summarizes key thermodynamic data. Fig. 7 illustrates the determination of the formation enthalpies  $\Delta H_f$  of MT–PA cocrystal. To obtain  $\Delta H_f$ , we integrate the heat-flow data of MT–PA cocrystal and the corresponding physical mixture of the component crystals (Fig. 7) from a common liquid-state temperature (130 °C) down to a common solid-state temperature (25 °C). The enthalpy of the cocrystal relative to the physical mixture is its formation enthalpy. For this system,  $\Delta H_f$  is  $-1.19 \text{ J}\cdot\text{g}^{-1}$  at 50 °C (the reaction is exothermic), indicating the cocrystal has a lower enthalpy than the physical mixture of component crystals. These negative enthalpy changes may also suggest a stabilization of the cocrystal compared to the components.

### Dissolution studies

Dissolution rate and apparent solubility of drugs are of paramount importance in pharmaceutical development and quality control, and shorter dissolution time and higher apparent solubility may result in more absorption. The powder dissolution profiles for MT, MT-PA cocrystal and the 1:1 MT/PA physical mixture in PBS (pH 6.8) are shown in Fig. 8a, in the form of the solution concentrations of MT ( $\text{mg}\cdot\text{mL}^{-1}$ ) vs. time (min). Compared with intact MT and the physical mixture, the cocrystal shows a higher solubility and a faster dissolution rate. The dissolution plot for MT-PA cocrystal reaches a maximum solubility ( $S_{\text{max}}$ ) within 20 min, which is followed by a decrease over time. This type of the “spring and parachute effect” has been exhibited by a lot of cocrystal systems recently.<sup>8,9</sup> The peak MT concentration of the cocrystal is roughly double that of API alone (Table 6). The supersaturated solution is formed at the initial stage of dissolution, and then preserved for several hours. Such a behavior is especially favorable for pharmaceutical applications. After 6 h, the concentration of MT-PA cocrystal is close to that of pure MT, indicating the cocrystal may slowly convert to MT accompanying the dissolution process, which was further confirmed by PXRD analysis of the remaining solids after the dissolution test.

Intrinsic dissolution rate (IDR) experiments were performed in order to obtain quantitative information on the dissolution rates.<sup>37</sup> The IDR results are graphed in Fig. 8b. All the samples demonstrate excellent linearity over the entire time span (60 min). The values obtained by least-squares analysis of the linear regions of the dissolution profiles are provided in Table 6. From these results an intrinsic dissolution rate of  $0.075 \text{ mg}\cdot\text{cm}^{-2}\cdot\text{min}^{-1}$  is obtained for the cocrystal, about 30% higher than that obtained for pure MT ( $0.058 \text{ mg}\cdot\text{cm}^{-2}\cdot\text{min}^{-1}$ ). In contrast, the physical mixture shows a comparable intrinsic dissolution rate to MT. This confirms the potential of this new cocrystal form to envisage new, more efficient formulations for MT. PXRD

analysis of the solids recovered after 60 min revealed that no phase transitions or crystallinity changes occurred during the intrinsic dissolution tests.

### **DVS studies**

Since the MT-PA cocrystal converted to MT after 6 h exposure to liquid water during the powder dissolution experiments, the disproportionation may also give rise to solid-state physical stability concerns. Thus the advantage of increased solubility and dissolution rate that the cocrystal provides must be considered relative to this potential stability disadvantage. Dynamic vapor sorption is a well-established method for the measurements of water vapor sorption and desorption of drug solids. Consequently, a DVS study was performed to investigate potential physical stability concerns. Dynamic vapor sorption and desorption isotherms for MT, MT-PA cocrystal and the 1:1 MT/PA physical mixture are shown in Fig. 9. It was evident that under all RH levels, MT-PA cocrystal sorbed more water than original MT, while less water than the physical mixture. The cocrystal is considered nonhygroscopic as it sorbs less than 0.08% water even at high humidity (90% RH) through sorption and desorption cycles. Further, the sorption-desorption curves are closed, suggesting no solid state transformation of cocrystals under the experimental conditions. Although the tendency of MT-PA cocrystal to convert to MT when exposed to water is not a desirable property from a processing point of view, the cocrystal is stable as an isolated solid and its kinetic stability under 0 ~ 90% RH levels is sufficient to allow standard processing steps to be used.

### **Conclusions**

A 1:1 cocrystal of MT with PA was obtained by a melt crystallization method with control of crystallization between 50 and 70 °C. Both crystal structure analysis and FTIR spectrum revealed the hydrogen bonding interactions occurred between amide group of MT and carboxylic acid group of PA in the cocrystal, and the formed hydrogen bonds were weaker than those in the component phases. The binary phase diagram established by DSC confirmed the ability of MT and PA to cocrystallize. The cocrystal melts at  $T = 80.6$  °C and the eutectic mixtures were identified at  $T = 71.1$  °C,  $\chi_{MT} \sim 0.37$ , and  $T = 78.9$  °C,  $\chi_{MT} \sim 0.65$ , respectively. The formation enthalpy for the cocrystal was  $-1.19$  J·g<sup>-1</sup> at 50 °C, indicating an enthalpic stabilization effect contributed to the cocrystallization. The DVS measurements confirmed that the cocrystal is nonhygroscopic under 0 ~ 90% RH levels as an isolated crystalline solid. For the cocrystal an approximate 2-fold increase in solubility and a 30% increase in intrinsic dissolution rate relative to MT indicate the potential of this new cocrystal form to envisage new, more efficient formulations for MT.

### Acknowledgements

Financial support from NSFC (grant no. 21101173, 91127002 and 21331007), NSF of Guangdong Province (S2012030006240), and Guangzhou Pearl River New Star Fund Science and Technology Planning Project (2013J2200054) is gratefully acknowledged.

## References

- 1 Ö. Almarsson, M. J. Zaworotko, *Chem. Commun.*, 2004, **17**, 1889-1896.
- 2 P. Vishweshwar, J. A. McMahon, J. A. Bis, M. J. Zaworotko, *J. Pharm. Sci.*, 2006, **95**, 499-516.
- 3 Guidance for Industry: Regulatory Classification of Pharmaceutical Co-Crystals. U.S. Department of Health and Human Services Food and Drug Administration Center for Drug Evaluation and Research. April 2013. Available from: <http://www.fda.gov/Drugs/GuidanceComplianceRegulatoryInformation/Guidances/default.htm>.
- 4 C. B Aakeröy, S. Forbes, J. Desper, *J. Am. Chem. Soc.*, 2009, **131**, 17048-17049.
- 5 A. V. Trask, W. Motherwell, W. Jones, *Int. J. Pharm.*, 2006, **320**, 114-123.
- 6 S. Karki, T. Frišćić, L. Fábián, P. R. Laity, G. M. Day, W. Jones, *Adv. Mater.*, 2009, **21**, 3905-3909.
- 7 Y. Yan, J. M. Chen, T. B. Lu, *CrystEngComm*, 2013, **15**, 6457-6460.
- 8 J. M. Chen, Z. Z. Wang, C. B. Wu, S. Li, T. B. Lu, *CrystEngComm*, 2012, **14**, 6221-6229.
- 9 S. L. Childs, L. J. Chyall, J. T. Dunlap, V. N. Smolenskaya, B. C. Stahly, G. P. Stahly, *J. Am. Chem. Soc.*, 2004, **126**, 13335-13342.
- 10 M. B. Hickey, M. L. Peterson, L. A. Scoppettuolo, S. L. Morrisette, A. Vetter, H. Guzmán, J. F. Remenar, Z. Zhang, M. D. Tawa, S. Haley, M. J. Zaworotko, Ö. Almarsson, *Eur. J. Pharm. Biopharm.*, 2007, **67**, 112-119.
- 11 D. P. McNamara, S. L. Childs, J. Giordano, A. Iarriccio, J. Cassidy, M. S. Shet, R. Mannion, E. O'Donnell, A. Park, *Pharm. Res.*, 2006, **23**, 1888-1897.
- 12 A. V. Trask, *Mol. Pharmaceutics*, 2007, **4**, 301-309.
- 13 D. R. Weyna, T. Shattock, P. Vishweshwar, M. J. Zaworotko, *Cryst. Growth Des.*, 2009, **9**, 1106-1123.
- 14 N. Rodriguez-Hornedo, S. J. Nehru, K. F. Seefeldt, *Mol. Pharmaceutics*, 2006, **3**, 362-367.
- 15 Takata N., Shiraki K., Takano R., Hayashi Y., Terada K., *Cryst. Growth Des.*, 2008, **8**, 3032-3037.
- 16 N. H. Chun, I. C. Wang, M. J. Lee, Y. T. Jung, S. Lee, W. S. Kim, G. J. Choi, *Eur. J. Pharm. Biopharm.*, 2013, **85**, 854-861.
- 17 I. C. Wang, M. J. Lee, S. J. Sim, *Int. J. Pharm.*, 2013, **450**, 311-322.
- 18 N. Shan, F. Toda, W. Jones, *Chem. Comm.*, 2002, **20**, 2372-2373.
- 19 S. Zhang, M. T. Harasimowicz, M. M. de Villiers, L. Yu, *J. Am. Chem. Soc.*, 2013, **135**, 18981-18989.
- 20 Yan Y., Chen J. M., Geng N., Lu T. B., *Cryst. Growth Des.*, 2012, **12**, 2226-33.
- 21 D. J. Berry, C. C. Seaton, W. Clegg, R. S. Harrington, S. J. Coles, P. N. Horton, M. B. Hursthouse, R. Storey, W. Jones, T. Frišćić, N. Blagden, *Cryst. Growth Des.*, 2008, **8**, 1697-1712.
- 22 K. Fucke, S. Myz, T. Shakhtshneider, E. Boldyreva, U. Griesser, *New. J. Chem.*, 2012, **36**, 1969-77.
- 23 D. X. Tan, L. C. Manchester, R. Hardeland, L. Silvia, C. M. Juan, M. S. Rosa, J. R. Russel, *J. Pineal. Res.*, 2003, **34**, 75-78.
- 24 H. Peng, F. Bouak, O. Vartanian, B. Cheung, *Int. J. Pharm.*, 2013, **458**, 156-168.

- 25 R. J. Reiter, *Best Pract. Res. Clin. Endocrinol. Metab.*, 2003, **17**, 273-285.
- 26 N. Buscemi, B. Vandermeer, R. Pandya, N. Hooton, L. Tjosvold, L. Hartling, G. Baker, S. Vohra, T. Klassen, Melatonin for treatment of sleep disorders. *Evidence Report/Technology Assessment* No. 108. Canada, 2004.
- 27 Circadin, melatonin. *European Public Assessment Report*. European Medicines Agency, 2007.
- 28 M. Vlachou, A. Eikosipentaki, V. Xenogiorgis, *Curr. Drug. Deliv.*, 2006, **3**, 255-265.
- 29 B. J. Lee, H. G. Choi, C. K. Kim, K. A. Parrot, J. W. Ayres, R. L. Sack, *Arch. Pharm. Res.*, 1997, **20**, 560-565.
- 30 B. J. Lee, K. A. Parrot, J. W. Ayres, R. L. Sack, *Int. J. Pharm.*, 1995, **124**, 119-127.
- 31 C. B. Aakeröy, D. J. Salmon, *CrystEngComm*, 2005, **7**, 439-448.
- 32 N. Qiao, M. Li, W. Schlindwein, N. Malek, A. Davies, G. Trappitt, *Int. J. Pharm.*, 2011, **1-2**, 1-11.
- 33 CrysAlisPro Version 1.171.35.19., Agilent Technologies Inc., Santa Clara, CA, USA, 2011.
- 34 G. M. Sheldrick, SHELXS 97, Program for Crystal Structure Refinement. University of Göttingen, Göttingen, 1997.
- 35 H. Yamashita, Y. Hirakura, M. Yuda, T. Teramura, K. Terada, *Pharm. Res.*, 2013, **30**, 70-80.
- 36 S. Zhang, I. A. Guzei, M. M. de Villiers, L. Yu, J. F. Krzyzaniak, *Cryst. Growth Des.*, 2012, **12**, 4090-4097.
- 37 D. J. W. Grant, T. Higuchi, *Solubility behavior of organic compounds*. New York, Wiley, 1990. Chapter XI.

**Table 1** The results of melt crystallization screen experiments with different cofomers

Coformer	MP /°C <sup>a</sup>	Screen results <sup>b</sup>
Glycolic acid	80	×
Glutaric acid	98	×
Oxalic acid	99	×
Pimelic acid	103	√
Mandelic acid	119	×
Benzoic acid	121	×
Malic acid	131	×
Cinnamic acid	134	×

<sup>a</sup> Melting point

<sup>b</sup> √: formation of new crystalline phase, ×: the physical mixture of MT and each coformer

**Table 2** The results of melt crystallization experiments at different MT/PA molar ratios and different holding temperatures after cooling the melt

Temperature <sup>a</sup>	Results <sup>b</sup>		
	2:1 MT/PA	1:1 MT/PA	1:2 MT/PA
RT	mixture	mixture	mixture
30 °C	mixture	mixture	mixture
40 °C	mixture	mixture	mixture
50 °C	cocrystal+MT	cocrystal	cocrystal+PA
60 °C	cocrystal+MT	cocrystal	cocrystal+PA
70 °C	cocrystal+MT	cocrystal	cocrystal+PA
80 °C	molten	molten	molten

<sup>a</sup> Room temperature (~25 °C), <sup>b</sup> mixture: physical mixture of MT and PA

**Table 3** Crystallographic data for MT-PA cocrystal

	MT-PA
<i>T</i> /K	150(2)
Wavelength /Å	1.54184
formula	C <sub>20</sub> H <sub>28</sub> N <sub>2</sub> O <sub>6</sub>
formula weight	392.44
crystal system	Monoclinic
space group	P2 <sub>1</sub> /c
<i>a</i> /Å	5.2497(3)
<i>b</i> /Å	49.977(2)
<i>c</i> /Å	7.6897(5)
<i>α</i> /°	90
<i>β</i> /°	104.573(6)
<i>γ</i> /°	90
<i>V</i> /Å <sup>3</sup>	1952.58(19)
<i>Z</i>	4
<i>D</i> <sub>calc</sub> /g·cm <sup>-3</sup>	1.335
<i>R</i> <sub>int</sub>	0.0314
GOF	1.123
<i>R</i> <sub>I</sub> , <i>wR</i> <sub>2</sub> [ <i>I</i> > 2σ( <i>I</i> )] <sup>a</sup>	0.0498, 0.1160
<i>R</i> <sub>I</sub> , <i>wR</i> <sub>2</sub> [all data] <sup>b</sup>	0.0623, 0.1225

<sup>a</sup>  $R_I = \frac{\sum ||F_o| - |F_c||}{\sum |F_o|}$ , <sup>b</sup>  $wR_2 = \frac{[\sum [w(F_o^2 - F_c^2)^2] / \sum w(F_o^2)^2]^{1/2}}{[\sum w(F_o^2 - F_c^2)^2]^{1/2}}$ ,  $w = 1/[\sigma^2(F_o)^2 + (aP)^2 + bP]$ , where  $P = [(F_o^2) + 2F_c^2]/3$

**Table 4** Hydrogen bond parameters for MT–PA cocrystal

D-H...A	D...A (Å)	D-H...A (°)
O3-H3...O1	2.575(2)	164(4)
O6-H6...O5 <sup>a</sup>	2.660(2)	172(3)
N1-H1...O3 <sup>b</sup>	3.209(3)	175(2)
N2-H2...O4 <sup>c</sup>	3.055	125

Symmetry codes: <sup>a</sup> -x+1, -y, -z+1, <sup>b</sup> 2 x-1, -y+1/2, z-1/2, <sup>c</sup> 1+x, 0.5-y, 0.5+z

**Table 5** Key thermodynamic data of MT, PA, and MT–PA cocrystal

Sample	MP /°C <sup>a</sup>	$\Delta H_m$ /J·g <sup>-1</sup>	$\Delta H_f$ /J·g <sup>-1</sup> <sup>b</sup>
MT	107.1	106.0	0
PA	117.3	172.5	0
MT–PA	80.6	131.8	- 1.19

<sup>a</sup> Melting point, <sup>b</sup>  $\Delta H_f$  is evaluated at 50 °C

**Table 6** Solubility and intrinsic dissolution rates for MT, MT–PA cocrystal, and 1:1 MT/PA physical mixture at 37 °C in PBS (pH 6.8)

Sample	Solubility /mg·mL <sup>-1</sup> <sup>a</sup>	IDR /mg·cm <sup>-2</sup> ·min <sup>-1</sup> /
MT	0.92	0.058
MT–PA	1.93	0.075
MT/PA mixture	0.94	0.061

<sup>a</sup> Maximum solubility at 20 min

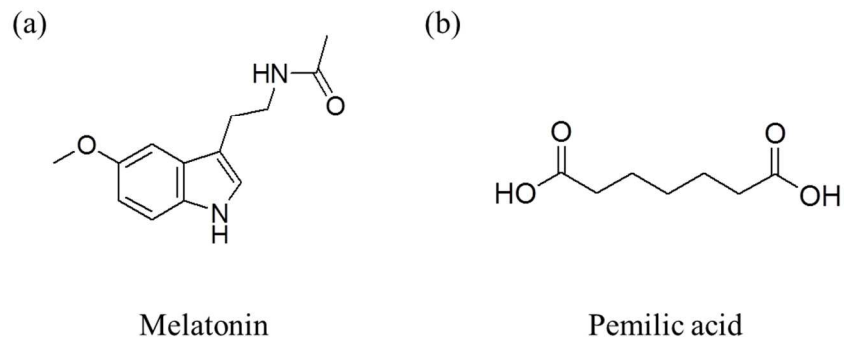


**Fig. 1** The structures of (a) MT and (b) PA.

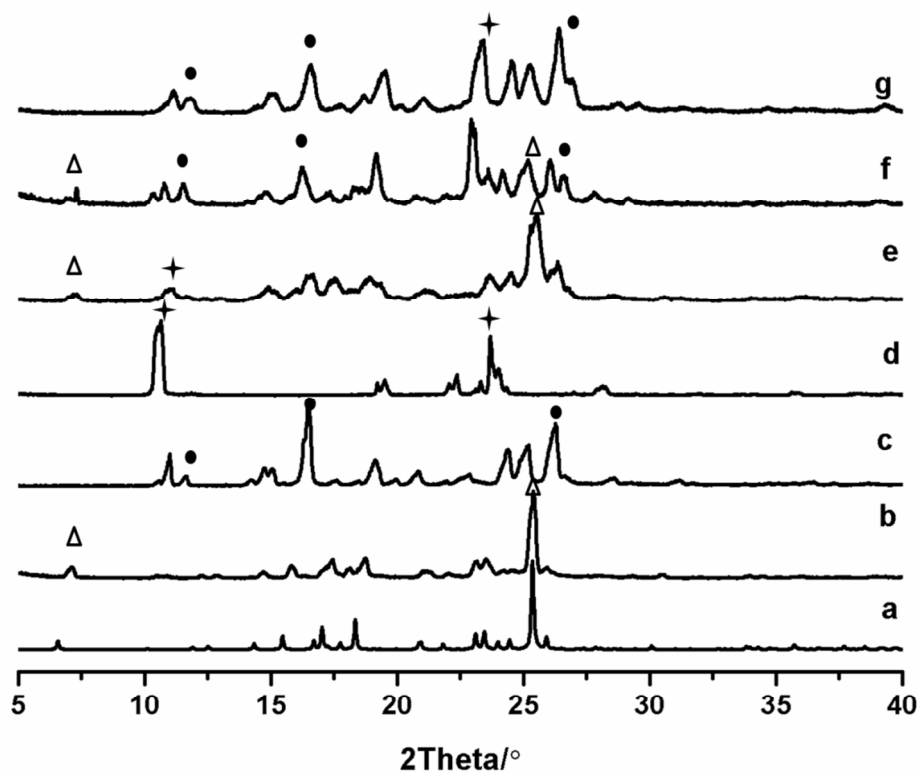


**Fig. 2** Comparison of PXRD patterns of MT-PA system: (a) MT-PA cocrystal (calculated); (b) 1:1 MT/PA crystallizing under 50 °C; (c) MT; (d) PA; (e) 1:2 MT/PA crystallizing under 50 °C; (f) 2:1 MT/PA crystallizing under 50 °C; (g) 1:1 MT/PA crystallizing under RT, In (b) bulk of powder is in good agreement with the pattern calculated from the single-crystal structure (a).

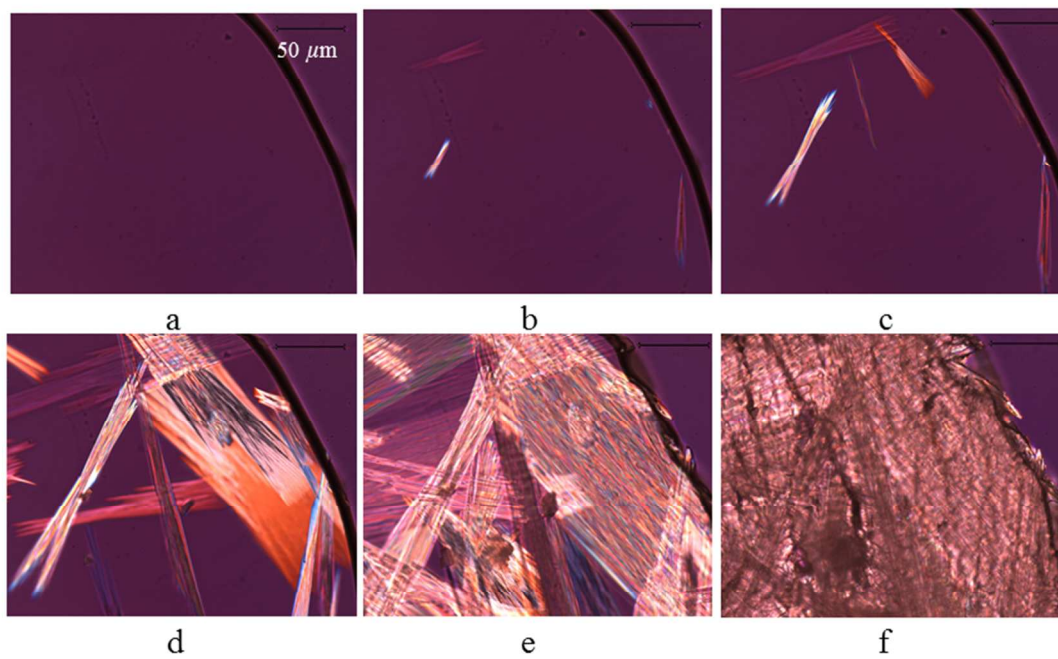


**Fig. 3** The crystallization behavior of the 1:1 molten mixture of MT/PA at 50 °C after (a) 0 min, (b) 10 min, (c) 12 min, (d) 30 min, (e) 4 h and (f) 10 h.

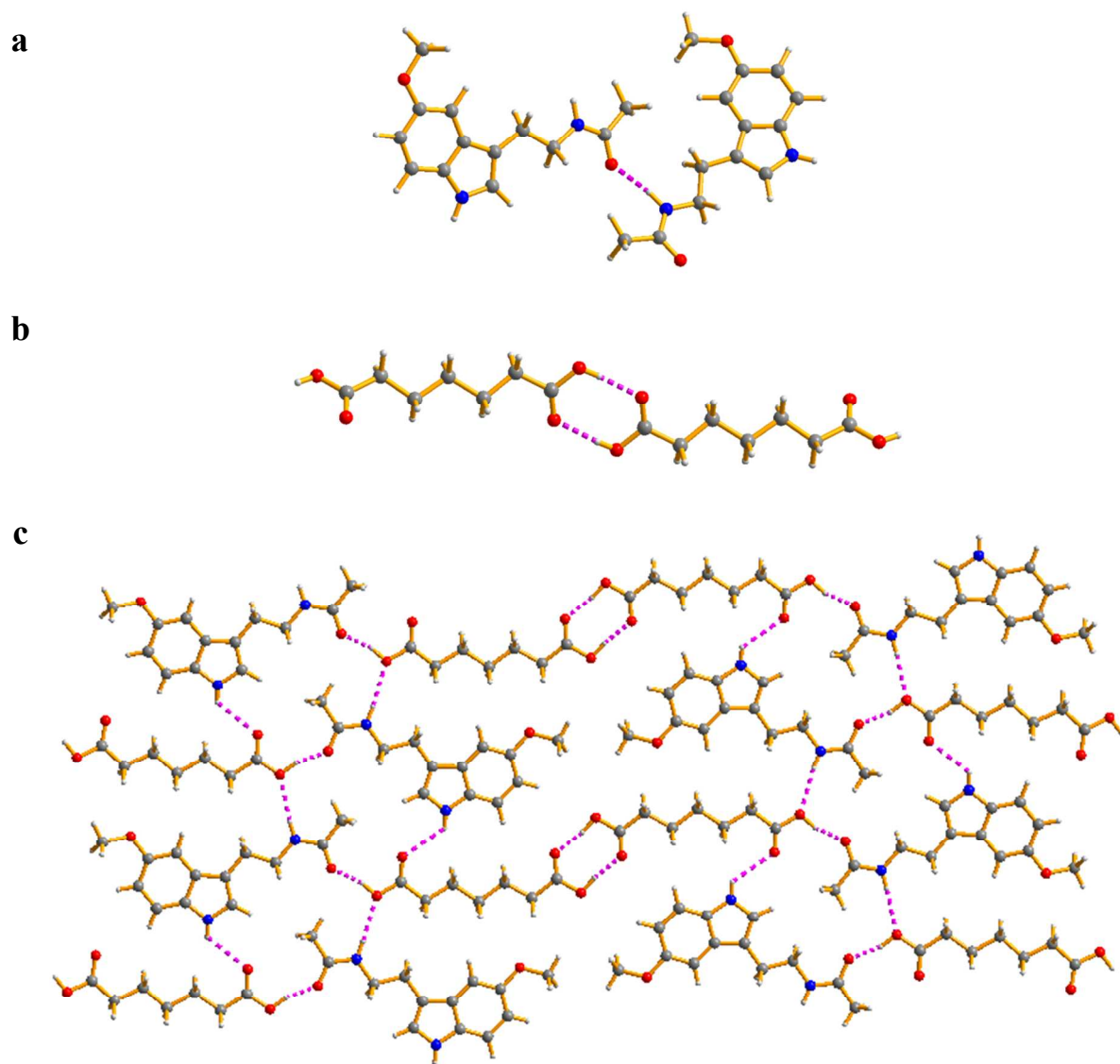


**Fig. 4** The crystal structures of (a) MT, (b) PA and (c) MT-PA cocrystal.

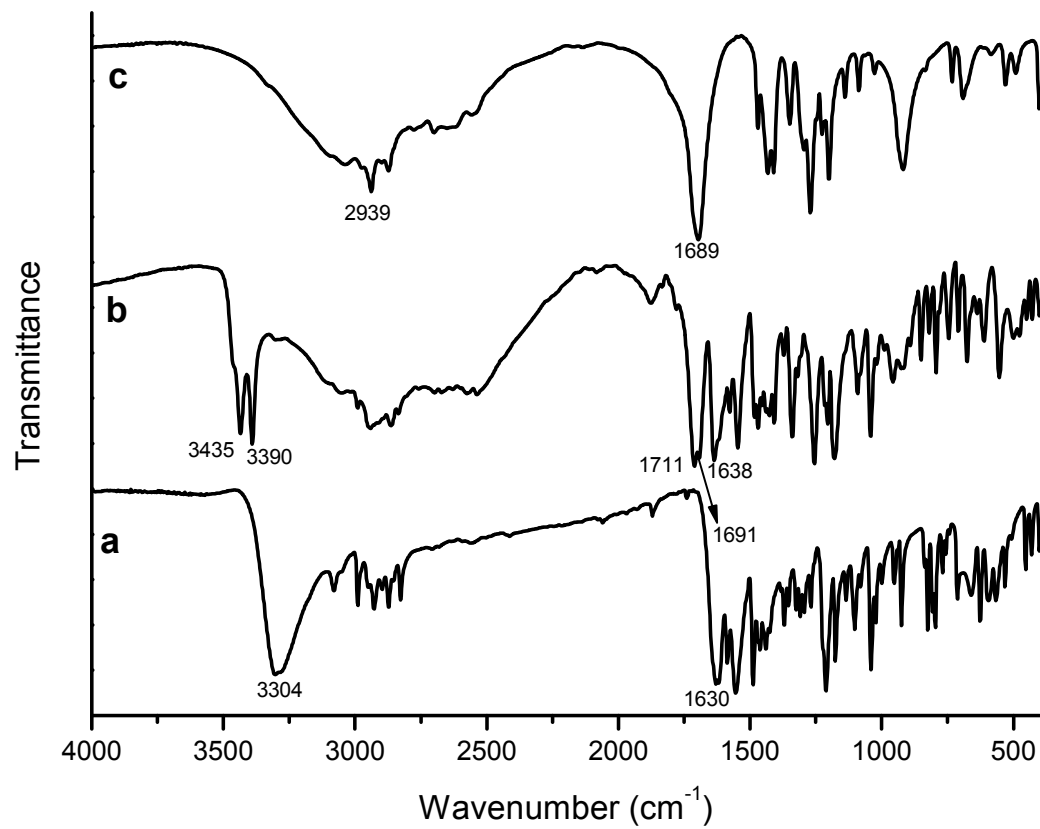
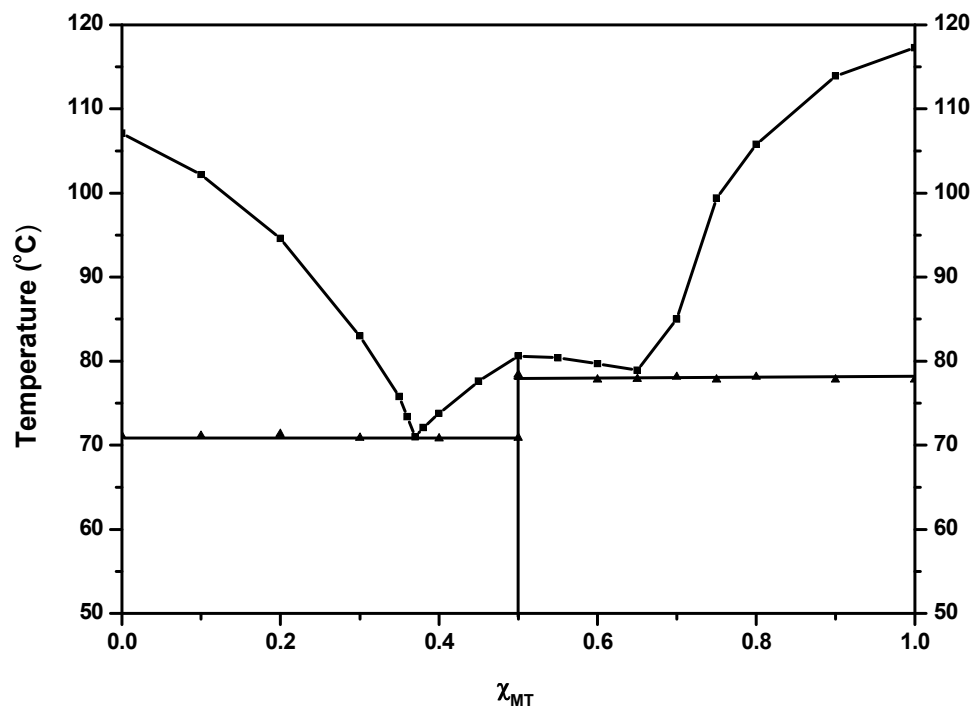
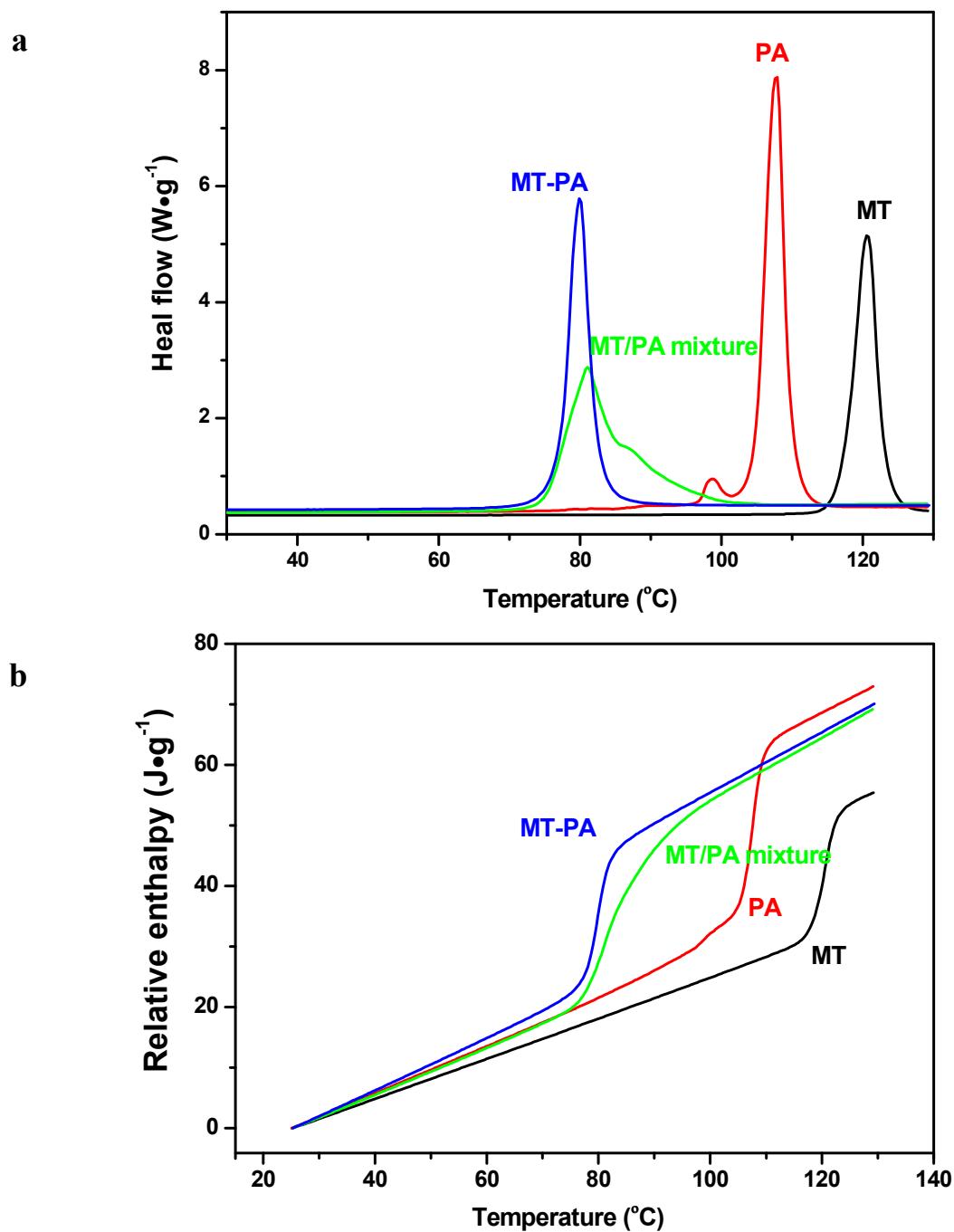


Fig. 5 FTIR spectra of (a) MT, (b) MT-PA cocrystal and (c) PA.



**Fig. 6** Temperature-composition phase diagram of MT-PA system.



**Fig. 7** (a) DSC melting endotherms of MT, PA, MT-PA cocrystal and 1:1 MT/PA physical mixture; (b) relative enthalpies between MT, PA, MT-PA cocrystal and 1:1 MT/PA physical mixture.

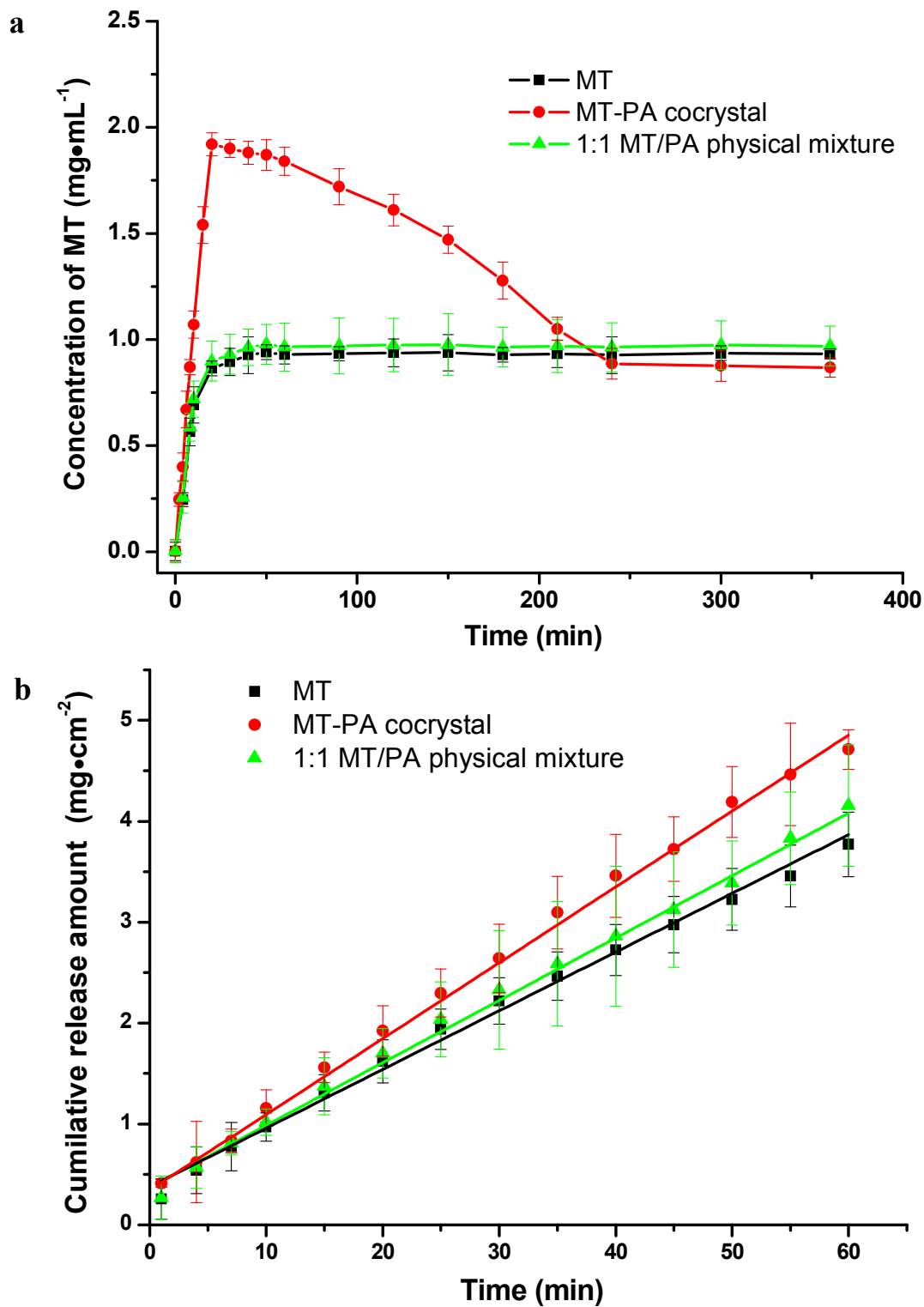


**Fig. 8** (a) Powder and (b) intrinsic dissolution profiles for MT, MT-PA cocrystal, and 1:1 MT/PA physical mixture in PBS (pH 6.8) at 37 °C.

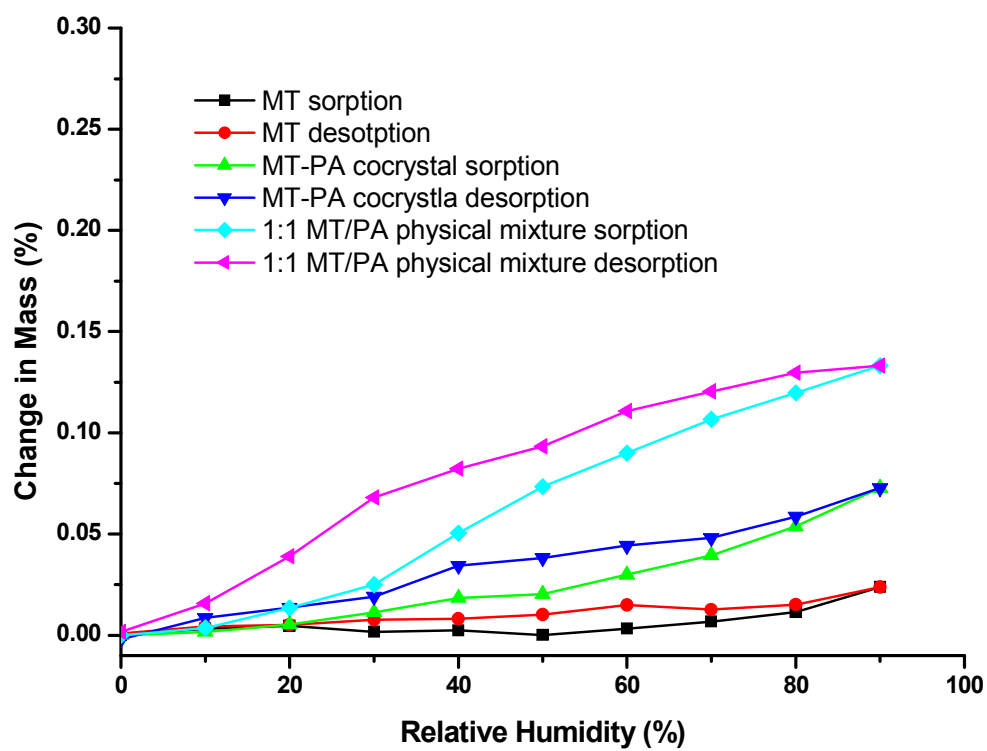
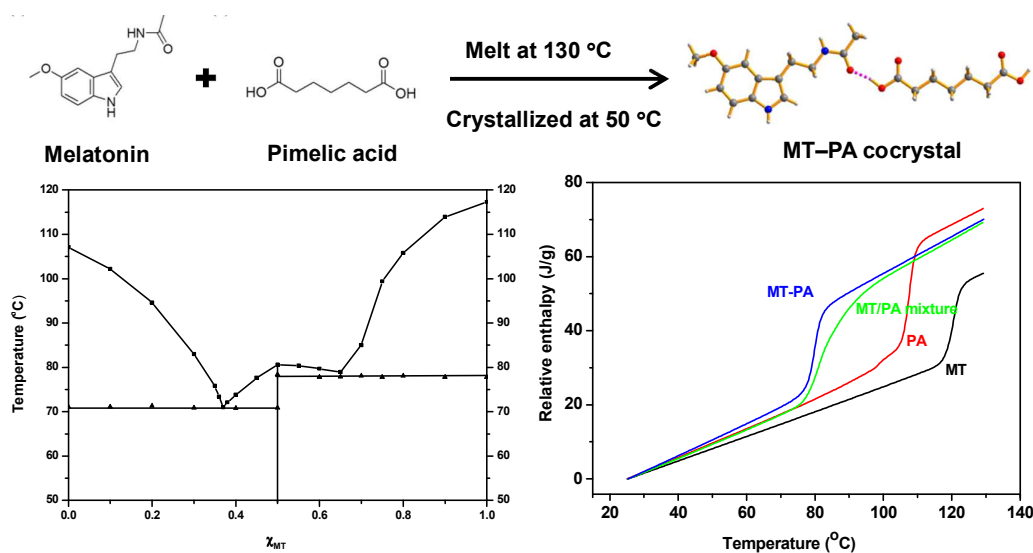


Fig. 9 DVS isotherm plots for MT, MT-PA cocrystal and 1:1 MT/PA physical mixture at 25 °C.

Thermodynamics and preliminary pharmaceutical characterization of melatonin–pimelic acid cocrystal prepared by a melt crystallization method

Yan Yan, Jia-Mei Chen, Tong-Bu Lu



Binary phase diagram and formation enthalpy provide in depth understanding and guidance for melt crystallization of melatonin–pimelic acid cocrystal.